Structural attributes and photo-dynamics of visible spectrum quantum emitters in hexagonal boron nitride

Supporting information

Nathan Chejanovsky [1,2], Mohammad Rezai [1], Federico Paolucci [2], Youngwook kim [2], Torsten Rendler [1], Wafa Rouabeh [2], Felipe Fávaro de Oliveira [1], Patrick Herlinger [2], Andrej Denisenko [1], Sen Yang [1], Ilja Gerhardt [1,2], Amit Finkler [1], Jurgen H. Smet [2] and Jörg Wrachtrup [1,2]

[1] 3. Physikalisches Institut, Universität Stuttgart, Pfaffenwaldring 57, 70569 Stuttgart, Germany

[2] Max Planck Institute for Solid State Research, Heisenbergstr. 1, 70569 Stuttgart, Germany

S1. Further structural examples

The flake in Fig. S1a was annealed in a Ar/H environment similar to Ref. 1. All other flakes in Fig. S1 were annealed at 850 °C.

In Fig. S1e a comparison is shown between an unfiltered/filtered confocal scan (left/right, respectively) for the chemical etching method using phosphoric acid. ‘Strip’ like structures

appear on the surface of the flake (marked in red rectangles) where emitters seem to be clustered around. In the example presented here, we also see that there is a constant angular dependence between the strips that appear, in this case $\alpha \sim n \times 60°$. The emitters are less organized in a line formation as in Fig. 1, leading us to believe that the etching reaction for chemical reasons is preferred on these perimeters. However, we have also seen that etching does not have to occur along straight lines. Further examples of angular multiplicity are seen for Figs. S1a, S1b, S1c.

Figure S1. Structural attributes on different flakes

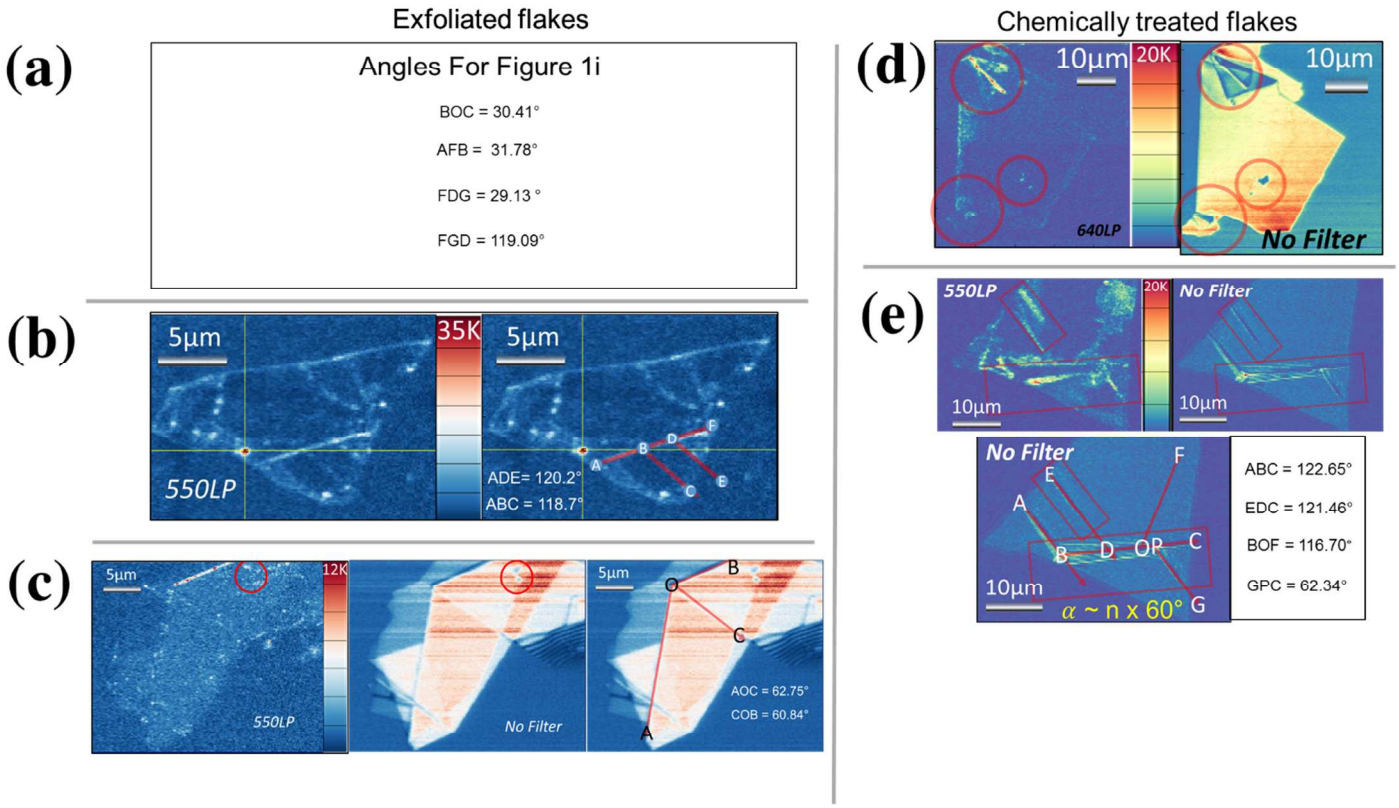

S2. SEM CVD monolayer h-BN structure

Figure S2 shows SEM images of graphene supermarket CVD h-BN residing on the copper foil. Three magnifications are seen, non-uniform coverage of the h-BN on the copper is evident.

Figure S2. SEM CVD monolayer h-BN structure

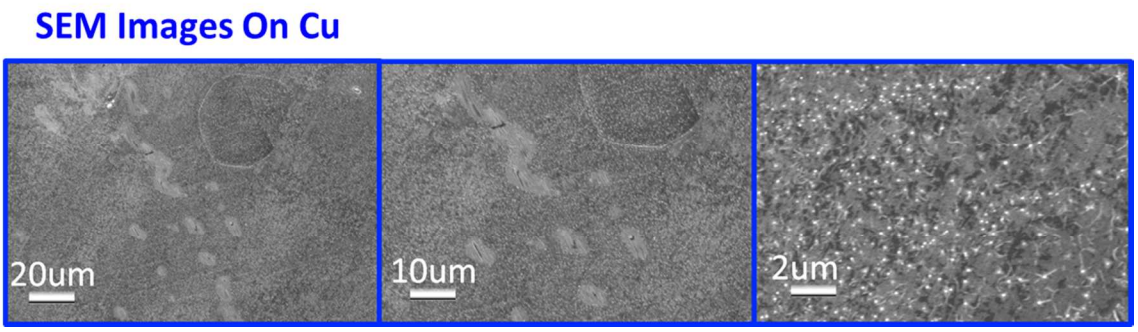

S3. Chemical testing and etching methods

Two chemical etching methods were used to create SQEs. We note for that the majority of the flakes to remain attached to the substrate it is important to anneal the sample first.

For the peroxymonosulfuric resistance test we first placed the sample inside H_2O_2:H_2SO_4 with a ratio of 3:7 at 135 ºC for 2 hours, which is known not to etch the h-BN.[2]

Etching method I (H_2O_2:H_2SO_4)

For mild etching of the flakes the sample was placed in H_2O_2:H_2SO_4 in a ratio of 3:6 at 135 ºC for 2 hours. The solution was let to cool down to room temperature and then diluted with distilled water (DI). Finally, the sample was rinsed in DI water, subsequently in isopropanol and dried with N_2 gas.

Etching method II (+H_3PO_4:H_2SO_4)

The sample was first mildly etched using etching method 1 for 20 minutes. After completion of method 1, the sample was placed in a solution of H_3PO_4:H_2SO_4 with a ratio of 1:8 at 75 ºC for 12 hours. The solution was then diluted with H_2O_2 mixed with DI water. Finally, the sample was rinsed in DI water, subsequently in isopropanol and dried with N_2 gas. This method is similar to the way h-BN functionalization was achieved as in Ref. 3.

These etching methods were tried both for diamond and SiO_2 substrates. For some samples we were able to work with emitters without annealing the sample after the etching procedure, but for increasing stability at the end of each etching method sample annealing at 850 °C in argon gas was beneficial, similar to the procedure in Ref. 4.

S4. Ion irradiation

Flakes were exfoliated on a patterned SiO_2 substrate in order to identify the flakes that were irradiated.

The sample was then annealed in vacuum to fixate the flakes to the SiO_2 substrate. Afterwards the sample was transferred to an irradiation chamber with a vacuum of $2 \cdot 10^{-7}$ mbar where homogeneous irradiation of He and N for predefined irradiation doses was done with acceleration energies of 2 keV and 2.5 keV, respectively. After irradiation the sample was annealed again at 850 °C in vacuum. Helium has been shown to convert BN from the hexagonal phase to the cubic phase. However, this was reported for much larger acceleration energies (> 200 keV) [5] far from our working range (<2.5 keV).

Figure S3 shows the PL spectra of high dose ion irradiation (10^{14} cm^{-2}), (left hand) for N (purple curve) and He (black curve). Comparing between both PL spectra we can deduce that the PL spectra is a superposition of many emitters. However, both PL spectra are not dissimilar and can be seen as a shift of one with respect to the other. Right hand of Figure 2c shows PL spectra for low dose irradiation. For both atom species a similar PL spectra is seen similar to that obtained from the untreated flakes and chemically treated flakes. Previous research using low energy Argon and N_2 ion irradiation (<2 keV) also suggests that the same defects were formed by both irradiation methods.[6] Due to the high density (Table 1) isolating SQEs in irradiated sample was more challenging.

Figure S3. Ion irradiation

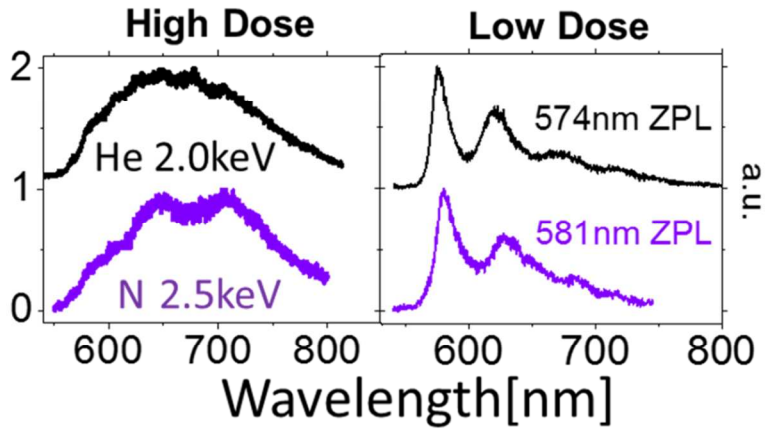

He and N implantation experiment in h-BN, High dose PL spectra is seen on the left side. As He/N implantation dose is reduced PL spectral features similar to untreated h-BN flakes and chemically etched flakes can be seen

S5. Emitter pair's excitation polarization comparison

In Fig. S4a we plot a QE's PL spectrum and superimpose autocorrelation measurements on the PL spectra for clarity. PL spectra (Fig. S4a) reveals a sharp peak in the wavelength regime of 550 nm to 575 nm. A closer look shows that it is constructed out of two peaks (Fig. S4a - inset). We fit this peak with two Lorentzians, which agrees well with the original peak. We associate the first two peaks with two zero phonon lines (ZPL). This is also confirmed by the autocorrelation measurement that goes to a value of $g^2(0) \sim 0.57$ (Fig. S4a-I), indicating it is *not a single QE*. We notice that the background also emits light in this wavelength (marked as 'background' in PL spectra), and therefore would contribute to our measured $g^2(0)$. Changing the spectrum detection range by filtering the PL spectrum on the APDs in the range of 575 nm to 600 nm assists in avoiding background contributions in an attempt to see if the value of $g^2(0)$ goes lower than 0.57. Indeed, $g^2(0)$ decreases to a value of 0.49 (Fig. S4a-II). We therefore conclude that the confocal spot contains two emitters. To better understand the spectral features, we perform cross-correlation measurements when filtering the spectrum on different parts for each APD: one in the range of 552 nm to 576 nm and the other one in the range of 640 nm and above (Fig. S4a-III). The value of $g^2(0)$ for this measurement is 0.66. We therefore conclude that the spectral features of both QEs are superimposed on the whole range of our spectral detection range. Asymmetric features appear on the cross correlation curve, which might indicate different excited states' lifetimes for each emitter.

If the emitters are associated with the h-BN structure, their dipole orientations should reflect the h-BN hexagon symmetry. Due to the possibility of various crystallinity of h-BN throughout a flake [7], the case presented above is a perfect test of two emitters in proximity at the same confocal spot.

To that end, we rotate the polarization of the excitation laser and record the PL spectrum. All spectral features of the emitter decrease in amplitude on the PL spectrum but retain their original PL shape as we rotate the linear polarization, and at 90 degrees a flat PL spectral line is recorded (Fig. S4b). It is therefore likely that both emitters are oriented in the same direction or with an angle of 180 degrees between them. A cartoon is depicted in Fig. S4b (inset) that approximates the angle of the linear polarization compared to the h-BN hexagonal ring when perpendicular to the emitter pair. Because the cross correlation measurement shows that the PL spectral features are overlapping and have a similar structure, it is more likely that a pair of defects of the same type are located on same site location on two different h-BN rings, which are inside our confocal spot.

More comparisons between excitation polarization angles for pairs of SQEs roughly in the range of ~5 μm from each other on the same flakes are seen in Fig. S4c, S4d and S4e. A difference of ~0 or approximately ~30 degrees between SQEs is seen (which would correspond to a 60 degree difference between sites on the h-BN hexagonal ring). We note that the polarization curves do not precisely overlap, perhaps due to curvature of the flake on the substrate which would lead to slightly different angles with the excitation laser between the SQE pairs.

Figure S4. Excitation Polarization

Two QEs on the same confocal spot

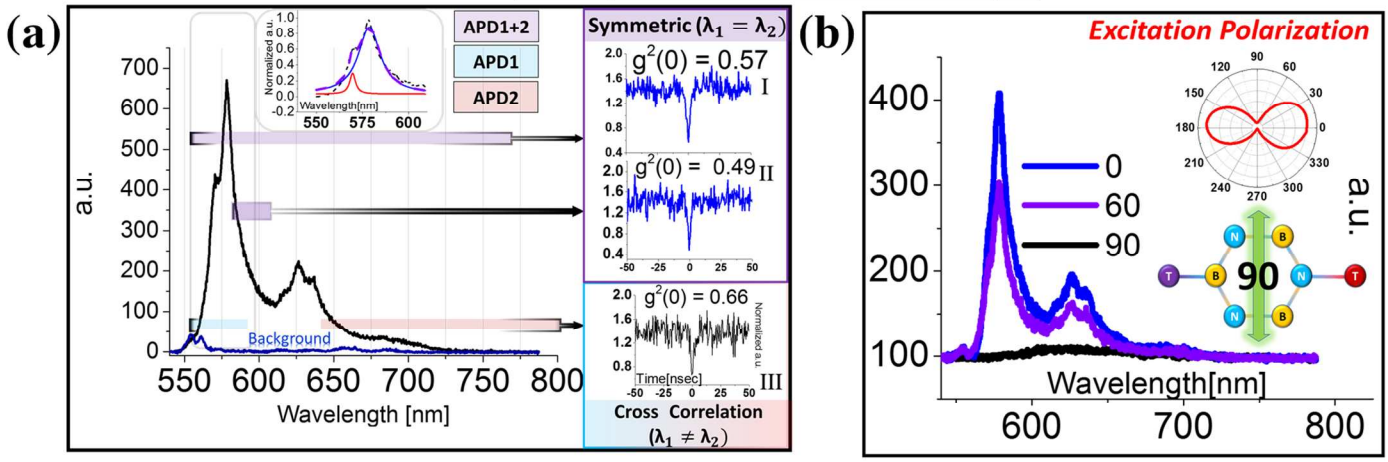

Excitation polarization for Two QEs on the same flake but different confocal spots

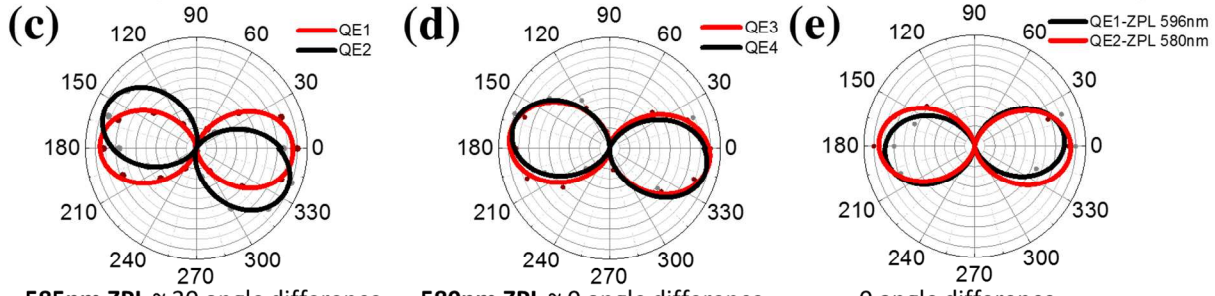

585nm ZPL ~ 30 angle difference

580nm ZPL ~ 0 angle difference

0 angle difference

S6. Chemical and gas environment treatments

To further exclude the source of the defects as external ad-atoms we also attempted to expose exfoliated flakes to different gas environments and different chemical environments. Firstly we anneal in Ar/H_2 gas environment at 350 °C as described in Ref. 1. Figure S5 shows that the associated PL spectra of the emitters with ZPLs in the range of 623 nm to 636 nm are still present after this treatment. h-BN is known for its high chemical inertness, whereas peroxymonosulfuric acid at certain concentrations is known not to harm h-BN during chemical cleaning, depending on acid concentrations.[2] To further clarify the origin of the defect we put the sample for 2 hours in an acid solution, after which we scan the flakes. Fig. S5 shows that QEs of ZPLs ranging from 586 nm to 593 nm are still present after the acid process.

Figure S5. PL Spectra after treatment

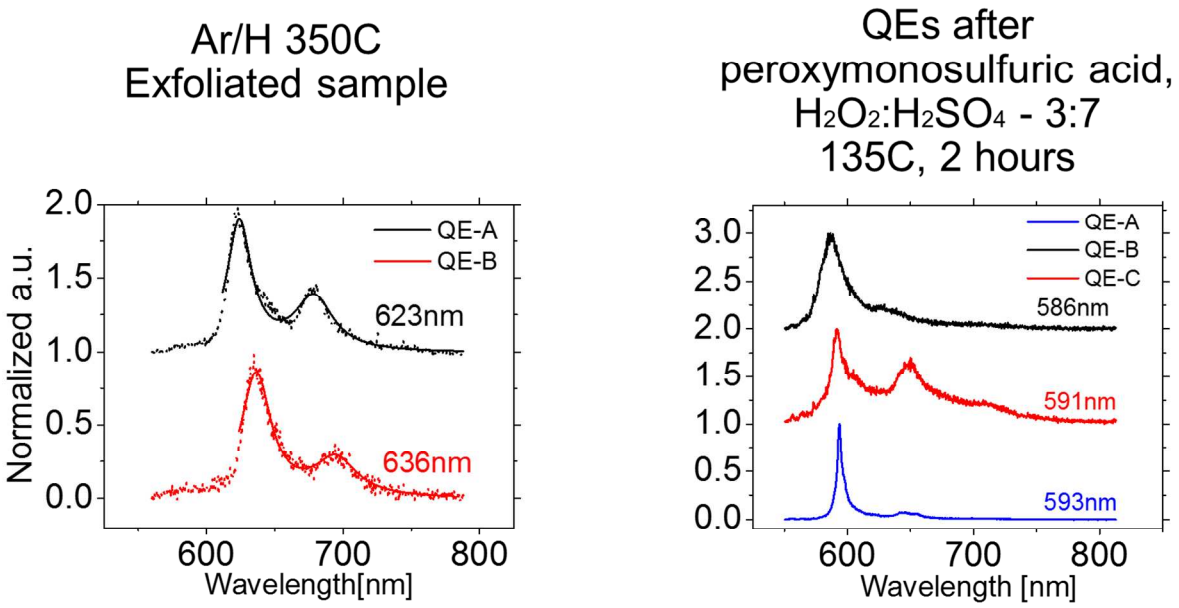

S7. In-house grown CVD h-BN

We examine in-house grown CVD h-BN on Cu foil and transfer it to SiO_2, sealing the sample in N_2 environment to avoid oxidation.[8] We probe the sample with a 532 nm laser with a power of 4.4 mW. We record a confocal image scan, PL spectra from two defects and auto-correlation measurement on a flake of micron scale (Fig. S6). Looking at the location of the defect in Fig. S6, it seems to be on a line shape on the h-BN flake, possibly indicating a surface perimeter.

PL spectra resemble those recently found in Ref. 9. We observe anti-bunching behavior. However, the emitter's $g^2(0)$ does not go below 0.5 with excited state time (for 4.4mW) τ_1 = 0.34 ns and metastable state time τ_2 = 402.35 ns. The background contribution to the signal is substantial and therefore we calculate the autocorrelation function after background subtraction [10]. After correction τ_1 = 4.37 ns. We note that after correction only one data point on the curve goes below 0.5. Considering our recent findings we note that by filtering one cannot exclude the spectral range of 550 nm to 575 nm as background since QE emission exists in this regime also as was shown in Fig. S4. We therefore tentatively attribute these features to a superposition of QEs which would result in a very short excited state lifetime.

Figure S6. In-house grown CVD h-BN

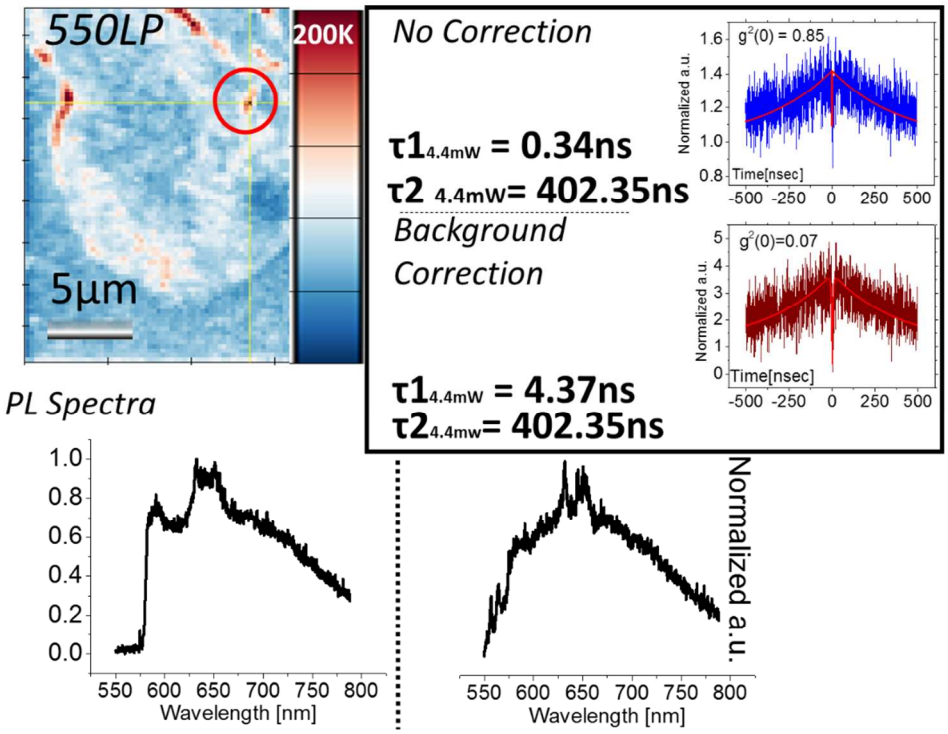

S8. Analysis of emitter with a ZPL of 580 nm from Fig. 2 in the main text

An example of the 580 nm ZPL emitter analyzed as a three level system is presented in the following using the equations from the main text. Fig. S7a displays the anti-bunching behavior, namely $g^2(t) < 1$ whereas in Fig. S7b the bunching behavior, $g^2(t) > 1$ (decaying 'shoulder' curves).

Figure S7. Analysis of emitter with a ZPL of 580nm from Fig. 2 in the main text

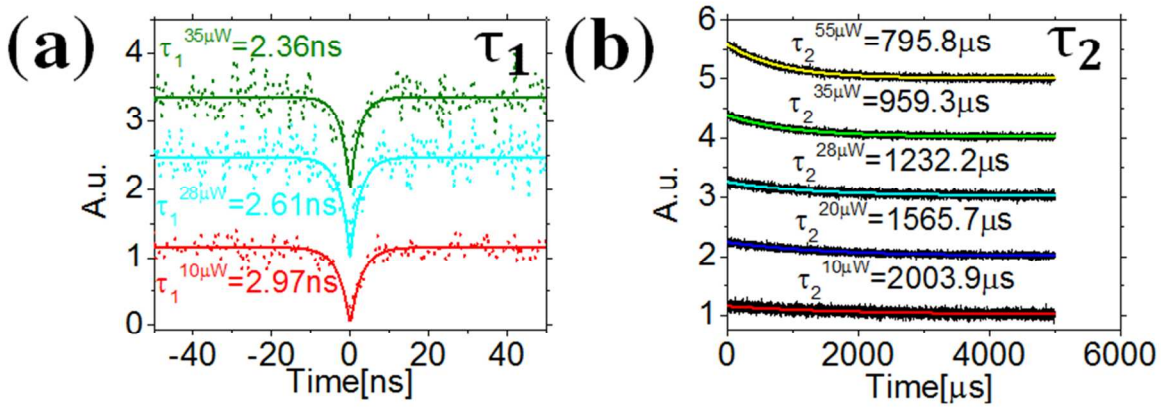

References:

(1) Wong, D.; Velasco, J.; Ju, L.; Lee, J.; Kahn, S.; Tsai, H.-Z.; Germany, C.; Taniguchi, T.; Watanabe, K.; Zettl, A.; Wang, F.; Crommie, M. F. *Nat. Nanotechnol.* **2015**, *10* (11), 949–953.

(2) Hui, W. C. *Proc. SPIE* **2004**, *5276*, 143–153.

(3) Bhimanapati, G. R.; Kozuch, D.; Robinson, J. *Nanoscale* **2014**, *6* (002), 11671–11675.

(4) Tran, T. T.; Bray, K.; Ford, M. J.; Toth, M.; Aharonovich, I. *Nat. Nanotechnol.* **2016**, *11*, 37–41.

(5) MacHaka, R.; Erasmus, R. M.; Derry, T. E. *Diam. Relat. Mater.* **2010**, *19* (10), 1131–1134.

(6) Peter, R.; Bozanic, a.; Petravic, M.; Chen, Y.; Fan, L. J.; Yang, Y. W. *J. Appl. Phys.* **2009**, *106* (8).

(7) Gibb, A. L.; Alem, N.; Chen, J. H.; Erickson, K. J.; Ciston, J.; Gautam, A.; Linck, M.; Zettl, A. *J. Am. Chem. Soc.* **2013**, *135* (18), 6758–6761.

(8) Museur, L.; Anglos, D.; Petitet, J. P.; Michel, J. P.; Kanaev, A. V. *J. Lumin.* **2007**, *127* (2), 595–600.

(9) Tran, T. T.; Zachreson, C.; Berhane, A. M.; Bray, K.; Sandstrom, R. G.; Li, L. H.; Taniguchi, T.; Watanabe, K.; Aharonovich, I.; Toth, M. *Phys. Rev. Appl.* **2016**, *5* (3), 2–6.

(10) Beveratos, a.; Kühn, S.; Brouri, R.; Gacoin, T.; Poizat, J. P.; Grangier, P. *Eur. Phys. J. D* **2002**, *18* (2), 191–196.